ESO Science Archive Facility - Phase 3 Data Release Description
ESO public survey programme KIDS - The Kilo-Degree Survey (VST), Data Release DR4.1
provided by K. Kuijken, submitted on 2020-04-17, published on 2020-05-20

ESO Phase 3 Data Release Description

Data Collection	KiDS
Release Number	4.1
Data Provider	Konrad Kuijken
Date	26.03.2020

Abstract

This data release constitutes the fourth public release by the Kilo-Degree Survey (KiDS). KiDS is an ESO public survey carried out with the VLT Survey Telescope and OmegaCAM camera, that will image 1350 square degrees in four filters (u, g, r, i), in single epochs per filter. KiDS was designed as a weak lensing shear tomography survey, and its core science drivers are mapping of the large-scale matter distribution in the universe and constraining the equation-of-state of Dark Energy. Additional science cases are manifold and range from galaxy evolution to Milky Way structure, and from detection of white dwarfs to high-redshift quasars.

This data release more than doubles the sky area covered by the first three releases combined, and for the first time includes photometry from the partner VIKING ESO public imaging survey on VISTA. For each of 1006 square-degree survey tiles the data release includes calibrated stacked images in u,g,r and i filters, their corresponding weights and masks, and single-band source lists extracted from the stacks. Furthermore, a multi-band ugriZYJHK$_s$ source catalogue is provided that encompasses the combined 1006 square degree area of this data release, with PSF-homogenised and aperture-matched photometry and photometric redshift estimates.

The VST data included in KiDS-ESO-DR4 were taken under ESO programme IDs: 177.A-3016(A), 177.A-3016(B), 177.A-3016(C), 177.A-3016(D), 177.A-3016(E), 177.A-3016(F), 177.A-3016(G), 177.A-3016(H), 177.A-3016(I), 177.A-3016(J), 177.A-3016(K), 177.A-3016(L), 177.A-3016(M), 177.A-3016(N), 177.A-3016(O), 177.A-3016(P), 177.A-3016(Q), 177.A-3016(S), 177.A-3017(A), 177.A-3018(A), 60.A-9038(A), and 094.B-0512(A). The VISTA data in this data release are taken from VIKING DR3 (q.v.), released Sept. 1, 2017.

This data release DR4.1 fixes a bug in the production of the DR4.0 catalogues. For a small fraction of sources, it resulted in erroneous MASK values for the NIR photometry from the VIKING survey. On 196 of the 1006 tiles, up to ~5% of the sources were affected. DR4.1 contains new multi-band catalogues as well as updated masks for these tiles. DR4.1 *ugri* images and single-band catalogues are identical to their DR4.0 counterparts.

The list of affected tiles is given in Table 9 at the end of this document. None of these changes affect data released as part of KiDS_DR3 or KIDS_DR3.1 .

With the corrected masks, the total unmasked area with valid 9-band photometry is increased by 0.5% with respect to DR4.

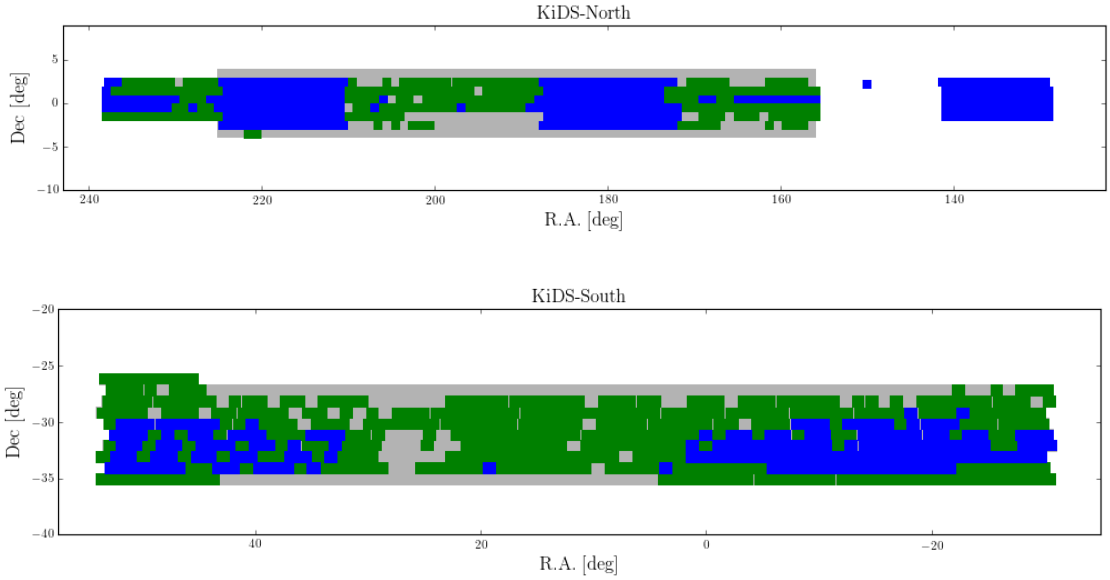

Figure 1: location of the 1006 KiDS-ESO-DR4 tiles. The area covered in DR1/2/3 is shown in blue, while the green tiles are new additions. The target 1350 sq.deg. KiDS survey area (top: KiDS-North; bottom: KiDS-South) is outlined in grey.

Overview of Observations

This data release (KiDS-ESO-DR4) consists of the coadded images, weight maps, masks and source lists of 1006 square degree survey tiles observed with OmegaCAM on the VST in u, g, r and i bands before January 24, 2018. It supercedes the 440 tiles released in DR1/2/3 (de Jong et al. 2015, A&A 582, A62; de Jong et al. 2017, A&A 604, A134). Figure 1 shows the DR4 footprint. Unlike the previous, incremental releases, for DR4 all data were reprocessed with improved astrometric and photometric calibration algorithms. The u,g,r and i images were reduced with the Astro-WISE system (McFarland et al. 2013, Exp.Astron., 35, 45).

In addition to these single-band data products, KiDS-ESO-DR4 includes a 9-band ugriZYJHKs source catalogue that spans all survey tiles in the data release. It contains list-driven, aperture- and PSF-matched GAaP photometry from the stacked VST images, as well as from the VISTA pointings taken for the near-IR VIKING survey (Edge et al. 2013, The Messenger 154, 32). The included sources are detected on a separate reduction of the r-band stacks with the THELI pipeline (Erben et al. 2013, MNRAS 433, 2545), optimised for the weak lensing analysis. These r-band detection images are also included in the data release.

From the beginning, KiDS and VIKING were conceived together as a combined survey, covering the same parts of the sky. The VIKING survey started before KiDS, and was terminated in 2015 before completing the originally planned 1500 square degree footprint. It was therefore decided that KiDS observations would prioritise the 1350 square degrees for which VIKING data exist. At the time of writing it seems likely that KiDS will also conclude observations once the 1350 square degree VIKING footprint has been covered. The footprint area shown in grey in Figure 1 is this reduced area.

Release Content

Imaging products and single-band source lists

The list of 1006 tiles for which imaging data products and single-band source lists are included in KiDS-ESO-DR4 is provided online at *http://kids.strw.leidenuniv.nl/DR4/data_table.php*.

Each tile was observed in u, g, r, and i band. The final footprint of each tile is slightly larger than 1 square degree due to the dithering scheme: 61.9x65.4 arcminutes in u; 62.3x66.8 arcminutes in g, r and i. Taking this into account, the total sky coverage is approximately **993** square degrees (1022 if the edges of the footprint, where there are fewer dither exposures, are included). Compared to previous DR the sky coverage of the released data is significantly more contiguous, as illustrated in Figure 1.
The single-band source lists were extracted from the calibrated, stacked images for each tile and filter separately, using the Astro-WISE processing system. In addition, a second, weak lensing-optimised reduction of the r-band survey tiles using the THELI data reduction pipeline was performed, resulting in a separate r-band source list that is used for the 9-band photometry and (future) weak lensing analysis (these catalogues are described in the next section).

Since the OmegaCAM CCD mosaic consists of 32 individual CCDs, the sky covered by a single exposure has gaps. In order to fill in these gaps, KiDS tiles are built up from 5 dithered observations in g, r and i and 4 in u. The dithers form a staircase pattern with dither steps of 25″ in X (RA) and 85″ in Y (DEC), bridging the inter-CCD gaps (de Jong et al., 2015, A&A, 582, A62). The tile centres are based on a tiling strategy that tiles the full sky efficiently for VST/OmegaCAM. Neighbouring dithered stacks have an overlap in RA of 5% and in DEC of 10%.

In Figure 2 the obtained seeing (FWHM), PSF ellipticity, and limiting magnitude (5σ AB in 2'' aperture) distributions per filter are shown, to illustrate the obtained data quality. In case of the filters observed in dark time (u, g, r) the FWHM distributions reflect the different observing constraints, with r-band taking the best conditions. Since i-band is the only filter observed in bright time, it is observed under a large range of seeing conditions. Average PSF ellipticities are always small: <0.1 (the average is over the absolute amount of ellipticity, regardless of the direction of ellipticity). The wide range of limiting magnitudes in i-band is caused by the larger range in seeing and in moon phase and thus sky brightness.

A repeat pass of the full KiDS area in i band is underway, and will be included in a future release. These new data do not suffer from the poor baffling of the VST in the period up to May 2015 that particularly affected the i band sky background.

For a full overview of the data quality parameters for each observation we refer to the following online table: *http://kids.strw.leidenuniv.nl/DR4/data_table.php*.

The single-band tiles in this data release consists of 19.114 files and a total data size of 179Gb of catalogue data and 17Tb of pixel data (image, weight and mask).

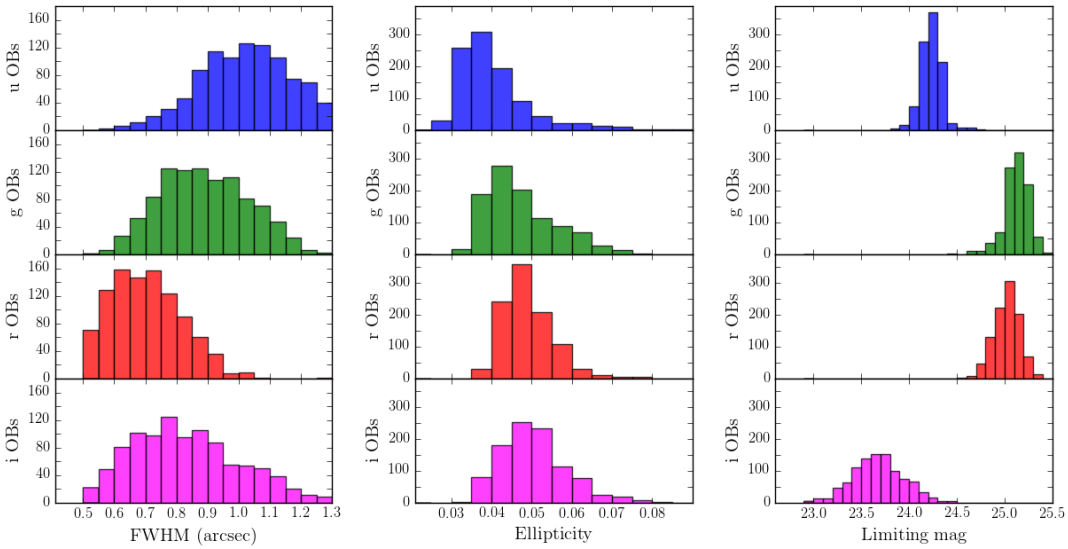

Figure 2: Tile-by-tile raw data quality parameters for KiDS-ESO-DR4. ***Left:*** *average PSF size (FWHM) distributions; centre****:*** *average ellipticity distributions (defined as 1-B/A, where A and B are the major and minor axis RMS length of the PSF);* ***right:*** *limiting magnitude distributions (5σ AB in 2'' aperture). The distributions are per filter: from top to bottom u, g, r, and i, respectively.*

9-band source catalogue

The KiDS-ESO-DR4 9-band source catalogue is based on the imaging data products described above, as well as new ZYJHK$_s$ near-IR photometry measured on the images from the overlapping VIKING survey on VIRCAM@VISTA. Here we provide a general description of the catalogue data, while an overview of all tiles with coordinates, PSF size, limiting magnitude, etc. is provided online: http://kids.strw.leidenuniv.nl/DR4/data_table.php.

The catalogue is based on the combined 1006 survey tiles, providing a total area coverage of approximately 1022 square degrees. The detection catalogue was generated from the r-band images reduced with the THELI pipeline. Those images form the basis for the weak lensing shape measurements, and this choice ensures that the definition of the sources in the photometric catalogue is consistent with the upcoming lensing catalogue (there was no such match between the DR3 photometric catalogue and the DR3.1 lensing catalogue, even though they were generated from the same raw data). The source coordinates and sizes were then used for forced (list-driven) 'Gaussian Aperture and PSF (GAaP)' photometry (Kuijken et al. 2015, MNRAS 454, 3500) on the Astro-WISE ugri VST images, and the ZYJHKs VISTA images reduced at the Cambridge Astronomical Survey Unit (CASU). The GAaP photometry for a source is effectively the integrated surface brightness over an elliptical Gaussian aperture function, defined on the intrinsic, seeing-deconvolved sky. It weights each part of the source consistently in each photometric band. Except for unresolved sources, it does not measure the total flux; instead the GAaP aperture size, shape and orientation it is optimised to return a high SNR flux for use in colour measurements. Error estimates on the GAaP fluxes are obtained by propagating the rms pixel noise through the measurement process.

The GAaP fluxes for the VST data were measured from the stacked u,g,r and i images. For the VISTA data, where the gaps between detectors are larger and PSF variations across the field and from subexposure to subexposure greater, photometry was measured from individual summed jittered 'paw-print' images (see VIKING DR3 release description). Each source was typically detected 2-6 times per near-IR filter, and the 9-band catalogue reports the optimally-weighted average flux over all available subexposures containing that source.

The initial photometric calibration of the VST images is based on nightly zeropoints from photometric standard star fields observations. These are subsequently refined at catalogue level with stellar-locus regression and anchoring to the Gaia G band photometry (Brown et al. 2018, A&A 616, A1). The flux scales in the images correspond to the nightly zeropoints, with the catalogue-level corrections reported in the image header.

VIKING imaging is calibrated to 2MASS photometry (Skrutskie at al. 2006, AJ, 131, 1163) within CASU. This calibration is verified after photometry is measured by comparing individual stellar flux estimates per paw-print to SDSS z-band data (Alam et al. 2015, ApJS 219, 12) for the Z-band, colour converted SDSS z and 2MASS J data for the Y-band, and 2MASS JHK data for the JHKs bands respectively. Median offsets between 2MASS and VIKING photometry per observation are also calculated, to flag poorly calibrated observations.

For any given source, GAaP photometry requires the same aperture to be specified across all bands, and this aperture must not be smaller than the seeing. The GAaP aperture radii are set to the rms radii measured on the r-band detection image (SExtractor parameters A_WORLD and B_WORLD), quadratically added to a minimum radius chosen to optimize the SNR. To accommodate occasional poor seeing in one of the 9 bands, GAaP photometry was run with two choices of a minimum Gaussian aperture rms radius: 0.7” and 1.0”. When the seeing is good in all bands the smaller setting will yield the most accurate measurements, and this photometry is used. But for a band where the seeing is poor, the larger aperture may yield a more accurate flux, or the smaller

aperture may not yield a flux measurement at all. The choice of aperture radius is made source by source.

A detailed description of the VIKING GAaP photometry is provided in Wright et al. (**ref**).

The 9-band catalogue contains a total of 100.350.873 sources, is made up of 1007 files (1006 data files and 1 metadata file), and has a total data volume of 28.5 GB.

Release Notes

Data Reduction and Calibration

The KiDS-ESO-DR4 pipeline is an evolution of the KiDS-ESO-DR3 pipeline (de Jong et al, 2017, A&A 604, A134) (DJ17) and based on the Astro-WISE optical pipeline described in McFarland et al. (2013, ExA 35, 45) (MF13). Below we summarize the processing steps and list KiDS-specific information (i.e., KiDS process configuration and departures from Astro-WISE optical pipeline). The main differences with the previous release are an improved astrometric calibration procedure, improved manual masking of satellite tracks, the separate r-band detection images produced with THELI that form the basis of the 9-band photometry catalogue, and the photometric calibration to the all-sky Gaia DR2 G band catalogue.

Image de-trending

De-trending of the raw data consists of the following steps.

- **Cross-talk correction**. Electronic cross-talk occurs between CCDs #93, #94, #95 and #96, resulting in faint imprints of bright sources on neighbouring CCDs. A correction was made for cross-talk between CCDs #95 and #96, where it is strongest (up to 0.7%).
- **De-biasing and overscan correction**. First, for each science and calibration exposure the overscan is subtracted per row (using method 6, see MF13). Second, a daily overscan-subtracted bias is subtracted. This is a daily average of 10 biases with 3σ-rejection.
- **Flat-fielding**. Whereas in the two previous data releases a single masterflat (per CCD and filter) was used for all data, changes to the telescope baffles in three steps during 2014/2015 necessitated the creation of new sets of masterflats. Table 1 lists the four different baffle configurations and the periods during which they were on the telescope.

Config.	Description	Start date	End date
1	Original set-up	May 2011	7 Jan 2014
2	Baffle extensions 1 (M2, chimney)	8 Jan 2014	6 Apr 2014
3	Baffle extensions 2 (M2, chimney, M1 plug)	7 Apr 2014	29 Apr 2015
4	Baffle extensions 3 (chimney ridges, plug)	30 Apr 2015	present

Table 1: VST baffle configurations

  For each baffling configuration a single masterflat (per CCD and filter) was used, by virtue of the stability of the intrinsic pixel sensitivities, that can be considered constant to ~0.2% or better for g, r and i (DJ15, Verdoes Kleijn et al., 2013, ExA, 35, 103). For g, r and i this master flat is a combination of a master dome (for high spatial frequencies) and master twilight (=sky) flat-field (for low spatial frequencies). Both contributing flats are an average of 5 raw flat-field exposures with 3σ-rejection. In u band only the twilight flats are used.
- **Illumination correction**. Illumination correction (a.k.a. "photometric superflat") is applied *in pixel space*, and only on the source fluxes (i.e., after background subtraction). A single illumination correction image is used to correct each masterflat (see also DJ15 and Verdoes Kleijn et al., 2013, ExA 35, 103). For baffling configuration 2, 3 and 4 illumination correction frames were derived from those for configuration 1, based on the difference between flatfields observed with each baffling configuration and with the original set-up.
- **De-fringing**. De-fringing is only needed for KiDS i-band. Analysis of nightly fringe frames showed that the pattern is constant in time. Therefore, a single fringe image was used for all KiDS-ESO-DR4 images observed after 2012-01-11. For each science exposure this

fringe image is scaled (after background subtraction of the science exposure and fringe frame) and then subtracted to minimize residual fringes.

- **Pixel masking.** Cosmic-rays, hot and cold pixels, saturated pixels are automatically masked as described in MF13 during de-trending. These are included in the weight image. Additional automatic and manual masking is applied on the coadds (see below).
- **Satellite track removal**. Satellite tracks are detected automatically by applying the Hough transform (Hough, 1962) to a difference image of maximally overlapping exposures within a dither sequence after masking bright stars and bright ghosts. The pixels affected by satellite tracks are masked and included in the weight image. Note: satellite tracks or parts thereof remaining after this automated step are masked during the coaddition stage, see below.
- **Background subtraction**. To remove vignetting by bond wire baffling (Iwert et al. 2006, Proc. SPIE 6276, 62760A) in the focal plane, a row-by-row background subtraction method is used, before the background subtraction done by SWARP (see below). Note: strong vignetting is not fully removed with this method and is masked during the coaddition stage, see below.

The THELI reductions of the r-band images are grouped in two-week 'runs' and new calibration frames are derived for each run. This includes illumination corrections, master flats, and biases. A more detailed description of the THELI processing will be given in Erben et al. (in preparation)'.

Photometric calibration

The steps taken to calibrate the photometry are as follows.

- KiDS-ESO-DR4 photometric calibration starts with individual zero-points per CCD based on secondary standard field observations. The calibration deploys a fixed aperture (6.3 arcsec diameter) not corrected for flux losses, and uses SDSS DR8 PSF magnitudes of stars in the SA fields as reference. Magnitudes are expressed in AB in the instrumental photometric system (i.e., no colour corrections between the OmegaCAM and SDSS photometric system applied).
- Next, the photometry in the g, r, and i filters is homogenized across CCDs and dithers for each filter in each tile independently. For u-band this homogenization is not applied because the relatively small source density often provides insufficient information to tie adjacent CCDs together. This global photometric solution is derived and applied in three steps:

    1. From the overlapping sources across dithered exposures, zero-point differences between the dithers (e.g. due to varying atmospheric extinction) are derived.
    2. Zero-point differences between CCDs are calculated using all CCD overlaps between the dithered exposures. Steps 1 and 2 both apply a minimization algorithm (see Maddox et al. 1990, MNRAS, 246, 433).
    3. The zero-point offsets are applied to all CCDs w.r.t. an average zero-point valid for the night, derived from the nightly SA field observations. If no SA field observations are available for the night, default values are used instead.

    The above steps complete the photometric calibration of the image data and single-band source lists. A further homogenization of the photometry over the whole survey area is calculated using, and applied to, the multi-band source catalog, and is described below.

Astrometry, regridding and coadding

A global (multi-CCD and multi-dither) astrometric calibration is calculated per filter per tile. SCAMP (Bertin 2006, ASP Conf. Series 351, 112) is used for this purpose, with a polynomial degree of 3 over the whole mosaic, while an initial model is supplied to constrain the focal plane geometry. The (unfiltered) 2MASS-PSC (Skrutskie et al. 2006, AJ, 131, 1163) is used as astrometric reference catalogue.

SWARP is used to resample all exposures in a tile to the same pixel grid, with a pixel size of 0.2 arcseconds. After background subtraction the exposures are coadded using a weighted mean stacking procedure.

Masking residual satellite tracks and bond wire baffling features

Spurious features remaining in the coadded images are identified by visual inspection of 1500x1500 pixel 'thumbnails', at two levels of contrast, by a team of KiDS members. Missed or incompletely masked tracks that are caught at this stage are marked manually on thumbnail images, after which an automatic procedure identifies and masks the tracks in the correct subexposure(s).
Residual background features due to the bond wire baffles are flagged manually, triggering the creation of masks based on standard region files.
Individual CCDs showing electronic instability are also manually flagged and removed from the list of frames to be co-added.
Finally, using the updated masks, new stacks and corresponding weight images are produced.

Masking of bright stars

A stand-alone program dubbed Pulecenella v1.0 (DJ15) was developed to create masks for KiDS coadds, and is now embedded in the pipeline. It is an automatized procedure for mask creation completely independent from external star catalogues. An example of a detail of a mask is shown in Figure 3. Pulecenella detects the following types of critical areas, all related to bright stars:

- saturated pixels,
- spikes caused by diffraction by the mirror supports,
- readout spikes,
- reflection halos produced by the optics components (a central core halo, and up to three wider reflection halos with spatially dependent offsets, depending on the brightness of the star.

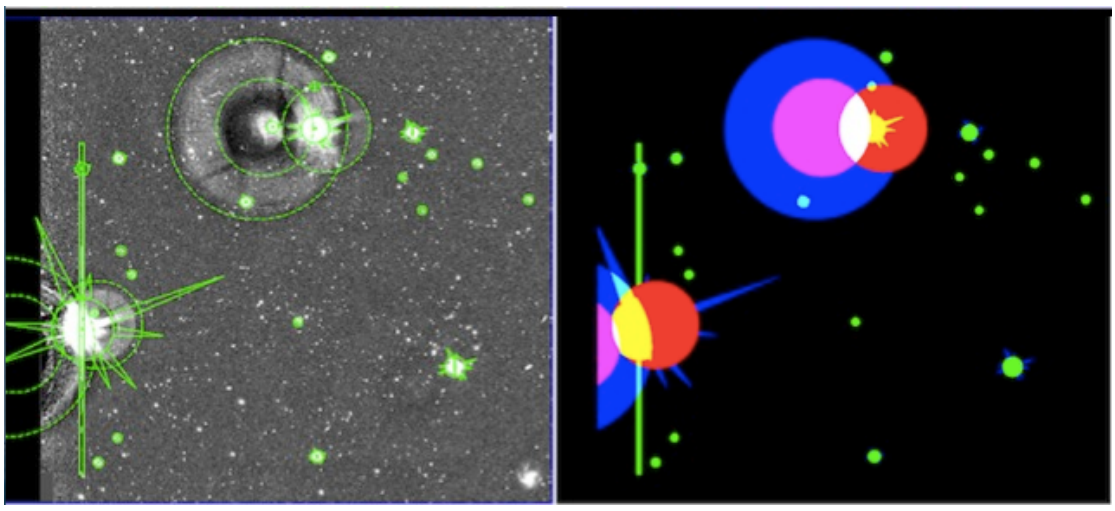

Figure 3: Detail of a Pulecenella v1.0 mask. ***Left:*** *detail of a KiDS stacked image with bright stars; critical areas detected by Pulecenella are over-plotted with green outlines.* ***Right:*** *FLAG image corresponding to the image shown on the left, with different colours indicating the pixel values resulting from the combination of different flag values.*

The masks are provided as FITS FLAG images, where each type of critical region is identified by a different flag value, as listed in Table 2. During source extraction for the single-band source list (see below) the FLAG image is used to flag sources whose isophotes overlap with the critical areas. The resulting flags are stored in the following two source parameters:

- IMAFLAGS_ISO: FLAG image flags OR'd over the isophote profile
- NIMAFLAG_ISO: number of flagged pixels entering IMAFLAGS_ISO

Type of area	Flag value	Type of area	Flag value
Readout spike	1	Secondary halo	16
Saturation core	2	Tertiary halo	32
Diffraction spike	4	Bad pixel	64
Primary halo	8		

Table 2: Critical areas in the single-band image masks and their flag values.

Parameter	Value	Description
DETECT_THRESH	1.5	<sigmas> or <threshold>,<ZP> in mag.arcsec-2
DETECT_MINAREA	3	minimum number of pixels above threshold
ANALYSIS_THRESH	1.5	<sigmas> or <threshold>,<ZP> in mag.arcsec-2
DEBLEND_NTHRESH	32	Number of de-blending sub-thresholds
DEBLEND_MINCONT	0.002	Minimum contrast parameter for de-blending
FILTER	Y	Apply filter for detection (Y or N)
FILTER_NAME	default.conv	Name of the file containing the filter
CLEAN	Y	Clean spurious detections? (Y or N)?
CLEAN_PARAM	1.0	Cleaning efficiency
BACK_SIZE	256	Background mesh: <size> or <width>,<height>
BACK_FILTERSIZE	3	Background filter: <size> or <width>,<height>
BACKPHOTO_TYPE	LOCAL	can be "GLOBAL" or "LOCAL"
BACKPHOTO_THICK	24	thickness of the background LOCAL annulus

Table 3: detection set-up for KiDS-ESO-DR4 single-band source lists

Single-band source list extraction and star/galaxy separation

The single-band source lists delivered in this data release are intended as "general purpose" source lists. Source list extraction and star/galaxy (hereafter S/G) separation is done with an automated procedure optimized for KiDS data: KiDS-CAT. This procedure, the backbone of which is formed by S-Extractor (Bertin & Arnouts, 1996, A&AS, 317, 393) performs the following steps.

1. S-Extractor is run on the stacked image to measure the FWHM of all sources. High-confidence star candidates are then identified (for details see La Barbera et al. 2008, PASP, 120, L681).
2. The average PSF FWHM is calculated by applying the bi-weight location estimator to the FWHM distribution of the high-confidence star candidates.
3. A second pass of S-Extractor is run with SEEING_FWHM set to the derived average PSF FHWM. During this second pass the image is background-subtracted, filtered and thresholded "on-the fly". Detected sources are then de-blended, cleaned, photometered, and classified. A number of S-Extractor input parameters are set individually for each image (e.g., SEEING_FWHM and GAIN), while others have been optimized to provide the best compromise between completeness and spurious detections (see the Data Quality section below). The detection set-up used is summarized in Table 3; a full SExtractor config file is available at this URL:
   http://kids.strw.leidenuniv.nl/DR4/example_config.sex
   Apart from isophotal magnitudes and Kron-like elliptical aperture magnitudes, a large number of aperture fluxes are included in the source lists. This allows users to estimate aperture corrections and total source magnitudes. All parameters provided in the source lists are listed in the Data Format section below.
4. S/G separation is performed based the CLASS_STAR (star classification) and SNR (signal-to-noise ratio) parameters provided by S-Extractor and consists of the following steps:

- In the SNR range where the high-confidence star candidates are located (the red dots in Figure 4) the bi-weight estimator is used to define their CLASS_STAR location, θ, and its width, σ; a lower envelope of θ − 4σ is defined.
- At SNR below that of the high-confidence star candidates, a running median CLASS_STAR value is computed from sources with CLASS_STAR > 0.8, which is shifted to match the θ − 4σ locus. The resulting curve (blue curve in Figure 4) defines the separation of stars and galaxies.

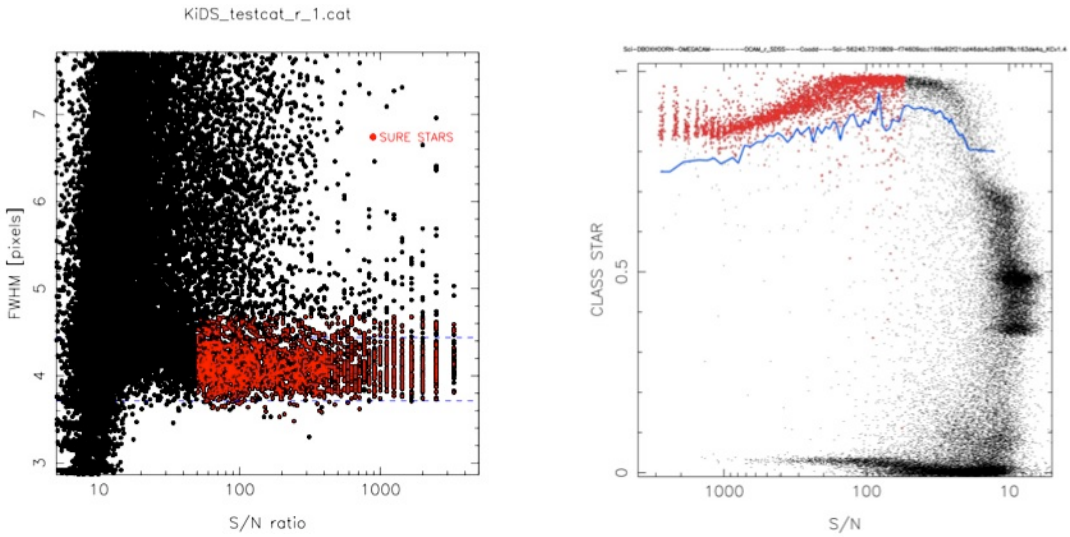

Figure 4: High-confidence star candidates and star/galaxy separation. ***Left:*** *the high-confidence star candidates (red dots) are used to locate the stellar locus and calculate the average FWHM of the image.* ***Right:*** *example of star/galaxy separation; at SNR >50, the high-confidence star candidates (red dots) are used to define the blue line; at lower SNR, all sources with CLASS_STAR>0.8 are used; sources above the blue line are classified as stars.*

The source magnitudes and fluxes in the final single-band source lists are not corrected for Galactic foreground or intergalactic extinction. The result of the S/G classification is available in the source lists via the 2DPHOT flag (SG2DPHOT in the multi-band catalog). Flag values are: 1 (high-confidence star candidates), 2 (objects with FWHM smaller than stars in the stellar locus, e.g., some cosmic-rays and/or other unreliable sources), 4 (stars according to S/G separation), and 0 otherwise (galaxies); flag values are summed, so 2DPHOT = 5 signifies a high-confidence star candidate that is also above the S/G separation line.

9-band source catalogue

Apart from the single-band VST data products, ESO-KiDS-DR4 also includes a matched-aperture photometry catalogue, containing 9 optical+near-infrared bands from a combined analysis of KiDS and VIKING. This catalogue is optimised for weak gravitational lensing science, and for this purpose an independent, high-accuracy astrometric analysis of the r-band images was performed using the THELI pipeline. Sources for the 9-band catalogue are detected on these 'detection images', and their positions used for list-driven photometry on the ugri KiDS and ZYJHKs VIKING 'science' images. The THELI-reduced r-band detection images, as well as their associated weight and mask images, are part of DR4. Accurate galaxy shape measurements for the galaxies will be provided as a separate data product in a further release.

Sources are detected on the THELI r-band detection images using SExtractor, and source aperture positions and sizes are then used to perform GAaP photometry on the KiDS (Astro-WISE) and VIKING (CASU) images. The detection setup is slightly different to the single-band Astro-

WISE setup in Table 3: the THELI setup uses DETECT_MINAREA=1, BACK_TYPE=MANUAL, BACK_VALUE=0.0,0.0 and DEBLEND_MINCONT=0.001*. Note that the sources in this catalogue are not necessarily the same as those in the single-band r-band source lists described above.* A number of morphological parameters are based on this SExtractor run, as well as GAaP fluxes, flux errors, and mask flags for each of the 9 bands. For each source the extinction in all nine filters is provided, interpolated from the extinction maps by Schlegel et al. (1998, ApJ, 500, 525), with updated extinction coefficients from Schlafly & Finkbeiner (2011, ApJ, 737, 103).

To prevent sources in tile overlaps from appearing multiple times in the catalogue, the survey tiles have been cropped to seamlessly connect to each other. Along the edges of survey tiles the data are less deep, but no worse than in the areas located in the gaps between the rows of CCDs in the focal plane, except along the outer edges of the contiguous areas. 9-band fluxes are reported for all r-band detections.

Seeing differences and aperture-matching

The catalogue includes magnitudes from the PSF homogenization and matched-aperture photometry "GAaP" pipeline. This novel technique is designed to account for PSF differences between different filters, while optimizing signal-to-noise. In short, the PSF within each coadded image is homogenized to a Gaussian shape without significantly degrading the seeing. Aperture photometry is then performed using elliptical Gaussian aperture weight functions, which are analytically corrected for seeing differences. A detailed description of the pipeline can be found in Kuijken et al. (2015, MNRAS, 454, 3500) (K15). It is important to note that these magnitudes are designed for deriving *accurate colours* of galaxies, not for total magnitudes of galaxies. For point sources (stars), GAaP magnitudes approach PSF-fitting photometry. The Gaussian aperture shape (Agaper,Bgaper) and orientation is set from the Sextractor A, B and PA measurements on the r-band detection image: Agaper=sqrt(MINAPER**2 + (A_WORLD*3600)**2), ditto B; values are maximised at MAXAPER=2". Photometry for two GAaP runs, with MINAPER=0.7" and 1.0", is reported in the catalogue (columns FLUX_GAAP_0p7_x and FLUX_GAAP_1p0_x, etc). The larger MINAPER value ensures valid measurements for those parts of the survey where the seeing in one of the bands was particularly poor.

Survey photometric homogenization

Zero-point corrections have been calculated for all ugri KiDS survey tiles included in the multi-band catalogue to improve the homogeneity of the photometry. These corrections are based on stellar locus regression (SLR). The SLR is used to calibrate the u, g and i filters to the r-band, and the latter is tied to Gaia DR2 using transformations derived from the overlap area between KiDS and SDSS.

The majority of stars display a well-defined photometric stellar locus: a tight relation in colour-colour space with a location that varies little across the sky outside the Galactic plane. SLR is the method where the observed stellar locus is matched to the fiducial intrinsic locus, and offers the possibility to achieve colour homogeneity. SLR was applied to the GAaP photometry of unmasked and not flagged, high S/N ($mag_{r,GAaP} < 19$) point sources ($0.4'' < FWHM_r < 0.8''$). Per source the GAaP magnitudes are corrected for Galactic extinction using the E(B-V) colour excess from Schlegel et al. (1998) and extinction coefficients from Schafly & Finkbeiner (2011). The stellar locus is parametrized using the "principal colours" *s*, *x* and *w* as defined by Ivezic et al. (2004, AN, 325, 583). For each of these colours (projections that are linear combinations of the ugri filters), a

straight section of the stellar locus lies parallel to one axis (P1) and is centred at 0 on the other axis (P2), see Fig. 5. We add a fourth, redundant colour *k* as additional guard for fitting robustness. Per source the P1 and P2 are calculated in each colour and sources on the straight part of the stellar locus are selected using fixed limits in P1. The median P2 values in each tile are converted to zero-point offsets with respect to r (d(u-r), d(g-r), d(i-r)). Fig. 5 shows an example of a typical fit.

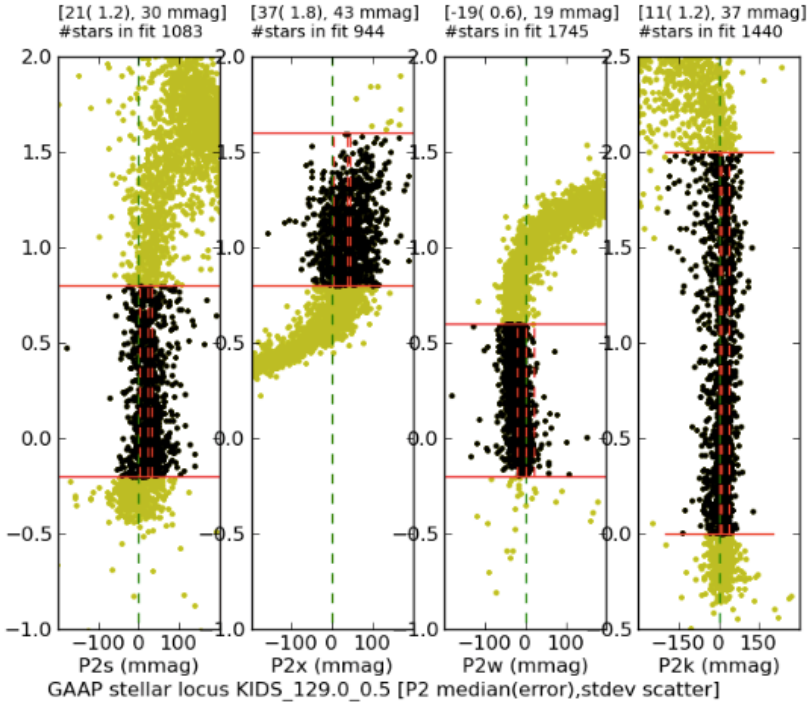

Figure 5: principal colours s,w,x and k for tile KiDS_129.0_0.5. The same stars (yellow) are plotted in each panel, with the stars used to locate the straight sections of the locus shown in black. The inferred median P2 offsets' formal errors and standard deviations are shown above each panel.

Already in DR3 we concluded that u band calibration with the SLR techniques described above resulted in large errors, and the alternative approach of overlap photometry was used. For DR4 a different approach was used for the u band, a combination of SLR with a latitude-dependent correction term, obtained by fitting the extinction-corrected u band as a function of dereddened (g-r) colour and galactic latitude over the SDSS region that overlaps with KiDS-N:

$u=g + 2.0(g-r)_0 + 0.456 + \max(0,0.66-2(g-r)_0) - 0.25\,|\sin(b)|$ $\quad (0.15<(g-r)_0<0.8)$

The u-band zeropoint of each KiDS tile is then adjusted until the median residual from this relation is zero.

The SLR yields a zero-point offset / correction per survey tile for each filter. The offsets as derived for band x are listed in the catalogue headers as Dx_SLR and Dx_SLR_1 for the MINAPER=0.7 and 1.0 GAaP runs. The offsets are also listed online in the catalogue table. By definition, the r-band SLR offset is zero.

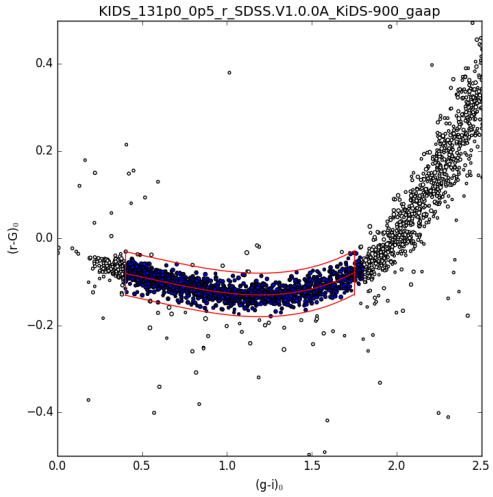

Figure 6. Illustration of the calibration of the r band photometry for tile KiDS_131.0_0.5 to the Gaia G band, using the dereddened KiDS (g-i) colours of stars with 16.5<G<19.25. The stars plotted in blue are used to determine the vertical location of the red box, which is centered on the relation derived from the SDSS-Gaia-KiDS overlap.

Calibration to Gaia-DR2 G band

With the advent of Gaia, a high-density, accurate photometric catalogue covering the whole sky has become available. Per tile typically 500-1000 Gaia stars were used to tie the r-band photometric zero point to the Gaia-DR2 G band calibration, using a fiducial dereddened (r-G) vs (g-i) colour-colour relation derived from the overlap of KiDS-North with the SDSS DR7 catalogue. The same offset is applied to u,g and i magnitudes as well, to preserve the SLR calibration. An example of this calibration is shown in Figure 6. These zeropoints are reported in the catalogue headers as DMAG_x and DMAG_x_1, for the MINAPER=0.7 and 1.0 GAaP runs, and are applied to the MAG_GAAP_0p7_x and MAG_GAAP_1p0_x magnitudes given in the catalogues. For each ugri image the zeropoint that is derived using the largest number of stars is recorded in the image header; the keyword CALMINAP records the corresponding value of MINAPER.

Near-infrared photometry from VIKING tied to 2MASS

VIKING photometry is calibrated to 2MASS during its processing. The GAaP fluxes in the 9-band catalogue use this calibration without change. All VIKING fluxes have magnitude zeropoint 30. More details are provided in Wright et al (2018).

Choice of GAaP aperture and extinction corrected magnitudes

Because the footprints of the VISTA and VST observations differ, the band-by-band seeing of the sources varies on scales smaller than a KiDS tile. The catalogue therefore provides a source-by-source choice between the MINAPER=0.7 and MINAPER=1.0 columns. The decision is based on the flux errors on the measurements of that source in all bands:

1. Define ERROR_RATIO_x = FLUXERR_GAAP_x_1p0 / FLUXERR_GAAP_0p7_x for each band x.
2. If MAX(ERROR_RATIO_x)*MIN(ERROR_RATIO_x) < 1, use the larger (1p0) aperture.

This choice ensures that the larger aperture is only used if, for at least one band, it yields a fractional improvement in flux error that is greater than the fractional penalty in any other band.

The fluxes that correspond to this best aperture choice are recorded in the catalogues as FLUX_GAAP_x, MAG_GAAP_x, etc. The magnitudes are corrected for the photometric zero-point and galactic extinction:

MAG_GAAP_x = DMAG_x – 2.5 log10(FLUX_GAAP_0p7_x) – EXTINCTION_x

or

MAG_GAAP_x = DMAG_x_1 – 2.5 log10(FLUX_GAAP_1p0_x) – EXTINCTION_x

where the DMAG_x and DMAG_x_1 values are those reported in the header for x=u,g,r,i, and equal to 30 for the VISTA Z,Y,J,H,Ks bands.

(Note that the magnitudes MAG_GAAP_0p7_x and MAG_GAAP_1p0_x are NOT corrected for extinction)

Extinction-corrected colours

In order to facilitate faster catalogue searches, the catalogue includes columns with source colours between adjacent bands (u-g, g-r, … , J-H, H-K_s). These colours are based on the GAaP magnitudes, which provide the most accurate colours both for galaxies and point sources. In these columns the zero-point corrections described above, as well as the per-source Galactic extinction corrections, are already applied.

Photometric redshifts

Based on the homogenized GAaP photometry, photometric redshifts have been calculated following the methods developed for CFHTLenS and described in K15. This makes use of the Bayesian photometric redshift code BPZ (Benítez, 2000, ApJ, 536, 571) in combination with the recalibrated templates from Capak (2004, PhD. thesis, Univ. Hawai'i). A new prior distribution (Raichoor A., et al., 2014, ApJ, 797, 102) has been used for DR4, which is more effective at fainter magnitudes than the prior used for DR3, but is biased by ca. +0.06 at bright magnitudes. We also switched to 68% confidence intervals for the photo-z posterior (previous releases reported 95%). **We caution all users that for accurate work, the photometric redshifts should be used in conjunction with external calibration data in order to quantify their error distribution** (see, e.g. Hildebrandt et al. 2017, 465, 1454)**.** The catalogue also includes the **ODDS** parameter, a measure of the uni-modality of the redshift PDF, and the best-fit template for each source (parameter T_B). The values correspond to the following types, where fractional types can occur because the templates are interpolated: 1=CWW-Ell, 2=CWW-Sbc, 3=CWW-Scd, 4=CWW-Im, 5=KIN-SB3, 6=KIN-SB2.

Data Quality

An overview of the intrinsic data quality of KiDS-ESO-DR4, in terms of seeing, PSF ellipticity, and limiting magnitudes distributions is presented in Fig. 2. In the following we focus on the quality of the reduced data products.

Photometric quality

The matter of photometric quality can be split up in two:

1. the uniformity of the photometry within each tile
2. the quality of the absolute photometric calibration per tile/filter

Both the internal photometric homogeneity within a coadd and the quality of the absolute photometric scale can be assessed by comparing the KiDS-ESO-DR4 photometry to SDSS DR8 (Aihara et al., 2011, ApJS, 193, 29). For this, PSF magnitudes were extracted from SDSS DR8 and compared to both the aperture-corrected and GAaP magnitudes in the KiDS-ESO-DR4 multi-band catalogue. Only stars with photometric errors both in KiDS and in SDSS smaller than 0.02 mag in g, r, and i or 0.03 in u were used. This comparison can be made only for all tiles in the KiDS-North field, but since KiDS-South was calibrated in the same way as KiDS-North, we expect the conclusions to hold for all data.

Figure 7 shows the offsets between KiDS aperture-corrected and SDSS DR8 magnitudes for 1 tile (KIDS_182.0_-0.5), which is a representative example. Generally, the photometry in a filter is uniform within one tile to within a few percent. In u-band the photometry may be less stable in some cases due to the lack of photometric homogenization within a tile.

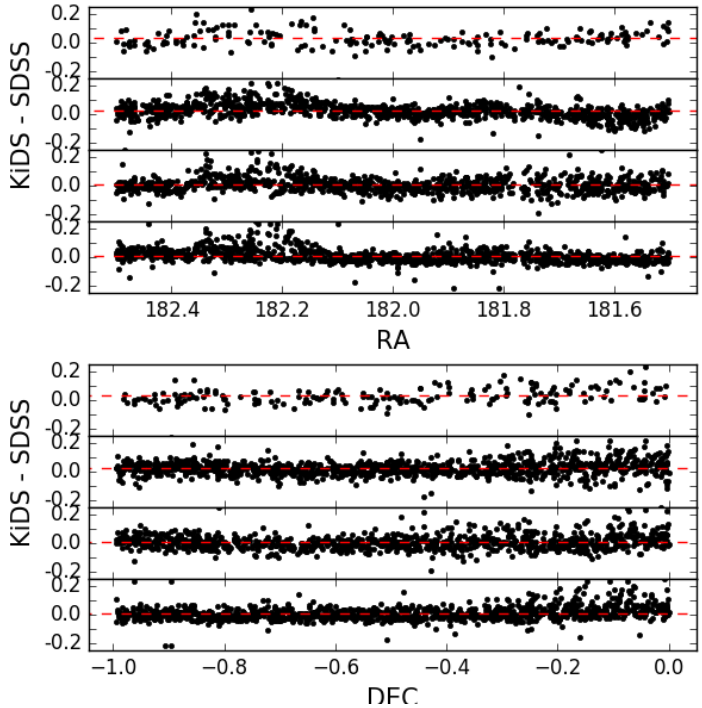

Figure 7: KiDS – SDSS magnitude offsets for (unmasked) stars in tile KiDS 182.0_-0.5 vs RA (top panel) and DEC (bottom panel), based on aperture-corrected fluxes. From top to bottom the sub-panels correspond to u, g, r, and i, respectively. Each dot corresponds to a star, and the red dashed lines indicate +0.05 and −0.05 magnitudes.

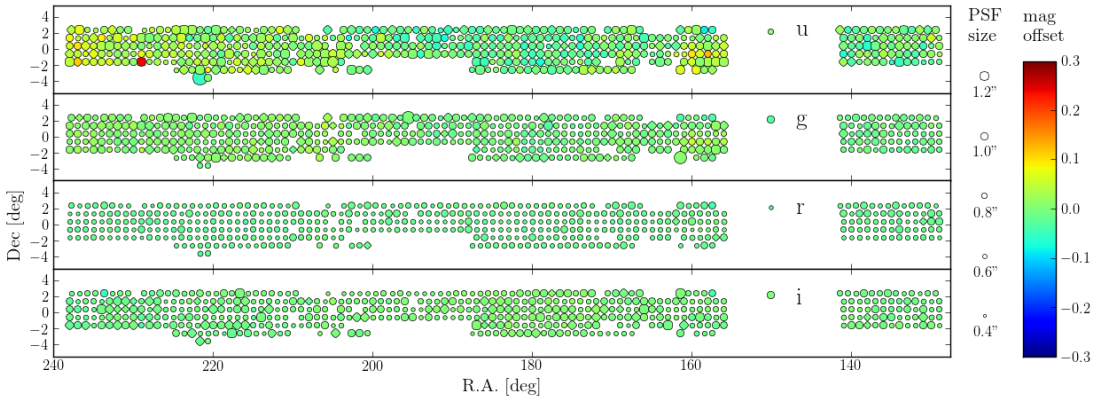

Fig. 8: Photometric calibration and PSF sizes in KiDS-North. Average magnitude offsets for KiDS-ESO-DR3 tiles between KiDS GAaP magnitudes and SDSS DR8 PSF magnitudes of stars are indicated by the colour coding, while the symbol size corresponds to the average PSF size.

The quality of the absolute photometric scale is illustrated in Figure 8 and summarized in Table 4. Small systematic offsets of 2 to 3 % are present in all filters. This could be due to the fact that nightly zero-points are determined using a fixed aperture on stars in the SA field without aperture correction. The scatter and occasional outliers in the standard calibration are due to non-photometric conditions (during either KiDS or SA field observations) and, particularly in case of the u-band, use of default zero-points for nights without good SA field observations. Photometric inhomogeneities in SDSS, which is reliable to 1% in gri and 2% in u (Padmanabhan et al. 2008, ApJ, 674, 2) also contribute to the measured scatter.

Filter	Mean offset (mag)	Standard deviation (mag)
u	0.008	0.035
g	0.001	0.014
r	-0.013	0.005
i	-0.003	0.009

Table 4: Average magnitude offsets and their standard deviation with respect to SDSS DR8 (for u,g,r,i) and expected stellar locus locations (in principal colours s,w,x) for GAaP and aperture-corrected (10'') magnitudes, both before and after photometric homogenization.

The photometric homogenization scheme significantly improves the stability of the calibration and annihilates the outliers completely, with the possible exceptions of isolated tiles or very small contiguous groups without photometric anchors. Derived using GAaP magnitudes, the homogenization clearly works best when applied to the GAaP magnitudes. Given the photometric stability of SDSS quoted by Padmanabhan et al. (2008, ApJ, 674, 2), the standard deviations of the offsets to SDSS (second to last column in Table 4) imply that the stability of the calibration in the u-, g- r- and i-bands is approximately 2%, 2%, 1% and 1%, respectively. Also when applied to the aperture-corrected magnitudes the stability of the calibration is significantly improved and outliers removed. The SLR step in the photometric homogenization procedure ensures that the stellar locus “principal colours” (bottom three rows in Table 4) are close to zero. Overall, the combination of GAaP magnitudes, extinction corrections and photometric homogenization produces the most accurate colours, both for stars and galaxies. Note that the colour columns in the multi-band catalogue already contain all these corrections, while the individual magnitude columns are not corrected for extinction and calibration variations!

Colour terms

The photometric calibration provided in KiDS-ESO-DR4 is in AB magnitudes in the instrumental system. We report here the colour-terms calculated with respect to the SDSS photometric system for DR3.

Aperture-corrected magnitudes taken from the multi-band catalogue, were matched to SDSS (DR8) PSF magnitudes of point-like sources. For each filter, the median offset to SDSS is first subtracted, rejecting tiles where this offset exceeds 0.1 mag in any of the g, r and i bands. The fit is made using all points from the remaining tiles. The resulting colour terms:

$$u_{KiDS} - u_{SDSS} = (-0.050 \pm 0.002)(u_{SDSS} - g_{SDSS}),$$
$$g_{KiDS} - g_{SDSS} = (-0.052 \pm 0.002)(g_{SDSS} - r_{SDSS}),$$
$$r_{KiDS} - r_{SDSS} = (-0.033 \pm 0.002)(g_{SDSS} - r_{SDSS}),$$
$$i_{KiDS} - i_{SDSS} = (+0.012 \pm 0.002)(r_{SDSS} - i_{SDSS}).$$

Known issues

Image defects

Scattered light and reflections

Some of the main issues in the DR1/2/3 VST/OmegaCAM data (before the baffling improvements described above were made) are related to scattered light and reflections. Due to the open structure of the telescope, light from sources outside the field-of-view can affect the observations. This expresses itself in a number of ways:

- Reflections: in some cases strong reflected light patterns are seen in the focal plane; these are caused by light from bright point sources outside the field-of-view and can occur in all filters.
- Vignetting by CCD masks: vignetting and scattering by the masks present at the corners of the focal plane array, and at the gaps between the rows of CCDs; this effect is particularly strong in i-band due to the bright conditions. The effect near the CCD gaps is largely corrected for, but in many cases the areas in the corners of the CCD array is strongly affected.
- Extended background artefacts: related to the reflections mentioned before, this is mostly seen in i-band and probably caused by moonlight.

Improvements to the telescope baffles that were installed in 2014 and 2015 significantly improved scattered light suppression. The i-band observations, many of which were taken with the moon above the horizon, were particularly affected by scattered light; a second i-band pass is underway and these new data (which will form part of DR5) should have significantly lower and smoother backgrounds.

More detailed illustrations of some of the scattered light effects are provided in the Release Notes accompanying KiDS-ESO-DR3.

Previous Releases

The current release, KiDS public data release number 4 or KiDS-ESO-DR4, was preceded by data release numbers 1-3 (KiDS-ESO-DR1/2/3). It supersedes these earlier releases, representing a complete re-reduction of all KiDS tiles completed before January 24th, 2018. For a small number of tiles the automatic reduction failed in a way that could not easily be fixed, and in order not to delay DR4 these have been excluded from the delivery. They will be included in DR5. These missing tiles include five tiles (KIDS_39.6_-34.1, KIDS_338.8_-32.1, KIDS_340.0_-32.1, KIDS_340.2_-31.2, KIDS_343.5_-32.1) which processed without error in DR1+2+3, but which failed to yield a consistent astrometric solution in the DR4 pipeline (conversely, a much larger number of tiles that gave problems in the earlier processing passed through the DR4 reduction without problem).

Apart from the large increase in area, from 440 to 1006 square-degree tiles, the main enhancement of DR4 over the previous release is the inclusion of the VIKING photometry in the multi-band catalogue, and the homogeneous calibration of the KiDS data to Gaia through stellar locus regression.

Data Format

Files Types

Table 5 lists the types of data products provided in this release, together with descriptions of the file types and naming conventions used.

The naming convention used for all data products is the following:

`KiDS_DR4.0_R.R_D.D_F_TTT.fits`,

where R.R and D.D are the RA and DEC of the tile centre in degrees (J2000.0) with 1 decimal place, F is the filter (u, g, r, or i for single-band data files, "ugriZYJHKs" for multi-band catalogue files), and TTT is the data product type (see column 4 of Table 5). **For those data products that were modified as part of DR4.1 the filename is changed accordingly, from KIDS_DR4.0_ to KIDS_DR4.1_ . This change affects the data products identified with (*) in Table 5, for the 196 tiles listed in Table 9.**

For example: the r-band stacked image of the tile "KIDS_131.0_-0.5" is called `KiDS_DR4.0_131.0_-0.5_r_sci.fits`.

Data product	ESO product category name	File type	TTT	F
Calibrated, stacked images	SCIENCE.IMAGE	FITS image	sci	u,g,r,i
Weight frames	ANCILLARY.WEIGHTMAP	FITS image	wei	u,g,r,i
Masks	ANCILLARY.MASK	FITS image	msk	u,g,r,i
Single-band source lists	SCIENCE.SRCTBL	Binary FITS table	src	u,g,r,i
Multi-band catalogue data file (*)	SCIENCE.MCATALOG	Binary FITS table	cat	ugriZYJHKs
THELI detection image	ANCILLARY.IMAGE	FITS image	det_sci	r
THELI weight image	ANCILLARY.IMAGE	FITS image	det_wei	r
Multi-band mask image (*)	ANCILLARY.MASK	FITS image	msk	ugriZYJHKs

Table 5: data products and file types. (*) see Table 9 for important note.

Format of coadded images

The final calibrated, coadded images from the Astro-WISE pipeline have a uniform pixel scale of 0.2 arcsec. The pixel units are fluxes relative to the flux corresponding to magnitude = 0, as based on nightly photometric calibrations. This means that the effective zero-point is equal to 0 and the magnitude m corresponding to a pixel value f is:

$$m = -2.5 \log_{10} f.$$

Subsequent photometric zeropoint corrections were derived from the catalogues and recorded in the image headers using the DMAG keyword. The keywords CALSTARS and CALMINAP give the number of Gaia stars that were used in the calibration, and CALMINAP is the value of the GAaP MINAPER parameter (0.7 or 1.0) that was used for the photometry that resulted in this zero-point.

The r-band detection images, which result from a reduction using THELI, specifically designed for optimal image shape measurement and small astrometric reductions, are the basis of the multi-band catalogue. They have a pixel scale that is closer to the native OmegaCAM pixel size of 0.213".

Catalogue Columns

Table 6 lists the columns that are present in the single-band source lists provided in KiDS-ESO-DR4. A large number (27) of aperture fluxes are provided to suit the needs of different users and allow interpolation to estimate e.g. aperture corrections. Only the columns for the smallest aperture (2 pixels, or 0.4 arcsec diameter) and the largest aperture (200 pixels, or 40 arcsec diameter) are listed in Table 6. Note: the label for the aperture of 28.5 pixels is FLUX_APER_28p5.

Table 7 lists the columns that are present in the multi-band source catalogue provided in KiDS-ESO-DR4. The meaning of the bits of the corresponding MASK values is explained in Table 8.

Table 6: columns provided in the KiDS-ESO-DR4 single-band source lists

Label	Format	Unit	Description
2DPHOT	J		Source classification
X_IMAGE	E	pixel	Object position along x
Y_IMAGE	E	pixel	Object position along y
NUMBER	J		Running object number
CLASS_STAR	E		S-Extractor S/G classifier
FLAGS	J		Extraction flags
IMAFLAGS_ISO	J		FLAG-image flags OR'ed over the iso. profile
NIMAFLAG_ISO	J		Number of flagged pixels entering IMAFLAGS_ISO
FLUX_RADIUS	E	pixel	Fraction-of-light radii
KRON_RADIUS	E	pixel	Kron apertures in units of A or B
FWHM_IMAGE	E	pixel	FWHM assuming a gaussian core
ISOAREA_IMAGE	J	pixel**2	Isophotal area above Analysis threshold
ELLIPTICITY	E		1 - B_IMAGE/A_IMAGE
THETA_IMAGE	E	deg	Position angle (CCW/x)
MAG_AUTO	E	mag	Kron-like elliptical aperture magnitude
MAGERR_AUTO	E	mag	RMS error for AUTO magnitude
ALPHA_J2000	D	deg	Right ascension of barycentre (J2000)
DELTA_J2000	D	deg	Declination of barycentre (J2000)
FLUX_APER_2	E	count	Flux vector within circular aperture of 2 pixels
...	...	...	...
FLUX_APER_200	E	count	Flux vector within circular aperture of 200 pixels
FLUXERR_APER_2	E	count	RMS error vector for flux within aperture of 2 pixels
...	...	...	...
FLUXERR_APER_200	E	count	RMS error vector for flux within aperture of 2 pixels
MAG_ISO	E	mag	Isophotal magnitude
MAGERR_ISO	E	mag	RMS error for isophotal magnitude
MAG_ISOCOR	E	mag	Corrected isophotal magnitude
MAGERR_ISOCOR	E	mag	RMS error for corrected isophotal magnitude
MAG_BEST	E	mag	Best of MAG_AUTO and MAG_ISOCOR
MAGERR_BEST	E	mag	RMS error for MAG_BEST
BACKGROUND	E	count	Background at centroid position

Label	Format	Unit	Description
THRESHOLD	E	count	Detection threshold above background
MU_THRESHOLD	E	arcsec**(-2)	Detection threshold above background
FLUX_MAX	E	count	Peak flux above background
MU_MAX	E	arcsec**(-2)	Peak surface brightness above background
ISOAREA_WORLD	E	deg**2	Isophotal area above Analysis threshold
XMIN_IMAGE	J	pixel	Minimum x-coordinate among detected pixels
YMIN_IMAGE	J	pixel	Minimum y-coordinate among detected pixels
XMAX_IMAGE	J	pixel	Maximum x-coordinate among detected pixels
YMAX_IMAGE	J	pixel	Maximum y-coordinate among detected pixels
X_WORLD	D	deg	Barycentre position along world x axis
Y_WORLD	D	deg	Barycentre position along world y axis
XWIN_IMAGE	E	pixel	Windowed position estimate along x
YWIN_IMAGE	E	pixel	Windowed position estimate along y
X2_IMAGE	D	pixel**2	Variance along x
Y2_IMAGE	D	pixel**2	Variance along y
XY_IMAGE	D	pixel**2	Covariance between x and y
X2_WORLD	E	deg**2	Variance along X-WORLD (alpha)
Y2_WORLD	E	deg**2	Variance along Y-WORLD (delta)
XY_WORLD	E	deg**2	Covariance between X-WORLD and Y-WORLD
CXX_IMAGE	E	pixel**(-2)	Cxx object ellipse parameter
CYY_IMAGE	E	pixel**(-2)	Cyy object ellipse parameter
CXY_IMAGE	E	pixel**(-2)	Cxy object ellipse parameter
CXX_WORLD	E	deg**(-2)	Cxx object ellipse parameter (WORLD units)
CYY_WORLD	E	deg**(-2)	Cyy object ellipse parameter (WORLD units)
CXY_WORLD	E	deg**(-2)	Cxy object ellipse parameter (WORLD units)
A_IMAGE	D	pixel	Profile RMS along major axis
B_IMAGE	D	pixel	Profile RMS along minor axis
A_WORLD	E	deg	Profile RMS along major axis (WORLD units)
B_WORLD	E	deg	Profile RMS along minor axis (WORLD units)
THETA_WORLD	E	deg	Position angle (CCW/world-x)
THETA_J2000	E	deg	Position angle (east of north) (J2000)
ELONGATION	E	deg	A_IMAGE/B_IMAGE
ERRX2_IMAGE	E	pixel**2	Variance of position along x
ERRY2_IMAGE	E	pixel**2	Variance of position along y
ERRXY_IMAGE	E	pixel**2	Covariance of position between x and y
ERRX2_WORLD	E	deg**2	Variance of position along X-WORLD (alpha)
ERRY2_WORLD	E	deg**2	Variance of position along Y-WORLD (delta)
ERRXY_WORLD	E	deg**2	Covariance of position X-WORLD/Y-WORLD
ERRCXX_IMAGE	E	pixel**(-2)	Cxx error ellipse parameter
ERRCYY_IMAGE	E	pixel**(-2)	Cyy error ellipse parameter
ERRCXY_IMAGE	E	pixel**(-2)	Cxy error ellipse parameter
ERRCXX_WORLD	E	deg**(-2)	Cxx error ellipse parameter (WORLD units)
ERRCYY_WORLD	E	deg**(-2)	Cyy error ellipse parameter (WORLD units)
ERRCXY_WORLD	E	deg**(-2)	Cxy error ellipse parameter (WORLD units)
ERRA_IMAGE	E	pixel	RMS position error along major axis

Label	Format	Unit	Description
ERRB_IMAGE	E	pixel	RMS position error along minor axis
ERRA_WORLD	E	deg	World RMS position error along major axis
ERRB_WORLD	E	deg	World RMS position error along minor axis
ERRTHETA_IMAGE	E	deg	Error ellipse pos. angle (CCW/x)
ERRTHETA_WORLD	E	deg	Error ellipse pos. angle (CCW/world-x)
ERRTHETA_J2000	E	deg	J2000 error ellipse pos. angle (east of north)
FWHM_WORLD	E	deg	FWHM assuming a gaussian core
ISO0	J	pixel**2	Isophotal area at level 0
ISO1	J	pixel**2	Isophotal area at level 1
ISO2	J	pixel**2	Isophotal area at level 2
ISO3	J	pixel**2	Isophotal area at level 3
ISO4	J	pixel**2	Isophotal area at level 4
ISO5	J	pixel**2	Isophotal area at level 5
ISO6	J	pixel**2	Isophotal area at level 6
ISO7	J	pixel**2	Isophotal area at level 7
SLID	K		Source list ID
SID	K		Source ID within the source list
HTM	K		Hierarchical Triangular Mesh (level 25)
FLAG	K		Not used

Table 7: Columns provided in the KiDS-ESO-DR4 9-band photometry catalogue

Label	Format	Unit	Description
General Source Parameters Derived from r-band THELI Detection Image			
ID	30A		ESO ID
SeqNr	1J		Running object number within the catalogue
SLID	1J		AstroWise Source list ID
SID	1J		AstroWise Source ID within the source list
FLUX_AUTO	1E	count	r-band flux (counts)
FLUXERR_AUTO	1E	count	Error on FLUX_AUTO (counts)
MAG_AUTO	1E	mag	r-band magnitude (mag)
MAGERR_AUTO	1E	mag	Error on MAG_AUTO (mag)
KRON_RADIUS	1E	pixel	Scaling radius of the ellipse for magnitude measurements
BackGr	1E	count	Background counts at centroid position (counts)
Level	1E	count	Detection threshold above background (counts)
MU_THRESHOLD	1E	mag*arcsec**(-2)	Detection threshold above background (mag arcsec^-2)
MaxVal	1E	count	Peak flux above background (counts)
MU_MAX	1E	mag*arcsec**(-2)	Peak surface brightness above background (mag arcsec^-2)
ISOAREA_WORLD	1E	deg**2	Isophotal area above analysis threshold (deg^2)
Xpos	1E	pixel	Centroid x position in the THELI image (pix)
Ypos	1E	pixel	Centroid y position in the THELI image (pix)
RAJ2000	1D	deg	Centroid sky position right ascension (J2000) (deg)
DECJ2000	1D	deg	Centroid sky position declination (J2000) (deg)
A_WORLD	1E	deg	Profile RMS along major axis (deg)
B_WORLD	1E	deg	Profile RMS along minor axis (deg)
THETA_J2000	1E	deg	Position angle (West of North) (deg)
THETA_WORLD	1E	deg	Position angle (Counterclockwise from world x-axis (deg)
ERRA_WORLD	1E	deg	World RMS position error along major axis (deg)
ERRB_WORLD	1E	deg	World RMS position error along minor axis (deg)
ERRTHETA_J2000	1E	deg	Error on THETA_J2000 (deg)
ERRTHETA_WORLD	1E	deg	Error on THETA_WORLD (deg)
FWHM_IMAGE	1E	pixel	FWHM assuming a gaussian object profile (pix)
FWHM_WORLD	1E	deg	FWHM assuming a gaussian object profile (deg)
Flag	1I		SExtractor extraction flags
FLUX_RADIUS	1E	pixel	Half-light radius (pix)
CLASS_STAR	1E		Star-galaxy classifier
GAaP photometry parameters from Astro-WISE co-added u,g,r,i images			
EXTINCTION_u	1E	mag	Galactic extinction in the u band (mag)
EXTINCTION_g	1E	mag	Galactic extinction in the g band (mag)
EXTINCTION_r	1E	mag	Galactic extinctio in the r band (mag)
EXTINCTION_i	1E	mag	Galactic extincion in the i band (mag)
Agaper_0p7	1E	arcsec	Major axis of GAaP aperture minaper 0.7arcs (arcsec)
Bgaper_0p7	1E	arcsec	Minor axis of GAaP aperture minaper 0.7arcs (arcsec)
Agaper_1p0	1E	arcsec	Major axis of GAaP aperture minaper 1.0arcs (arcsec)
Bgaper_1p0	1E	arcsec	Minor axis of GAaP aperture minaper 1.0arcs (arcsec)
PAgaap	1E	deg	Position angle of major axis of GAaP aperture (North of West) (deg)
FLAG_GAAP_0p7_u	1J		GAaP Flag for MAG_GAAP_u minaper 0.7arcs
FLAG_GAAP_0p7_g	1J		GAaP Flag for MAG_GAAP_g minaper 0.7arcs

FLAG_GAAP_0p7_r	1J		GAaP Flag for MAG_GAAP_r minaper 0.7arcs
FLAG_GAAP_0p7_i	1J		GAaP Flag for MAG_GAAP_i minaper 0.7arcs
FLUX_GAAP_0p7_u	1E	count	GAAP u-band flux minaper 0.7arcs (counts)
FLUX_GAAP_0p7_g	1E	count	GAAP g-band flux minaper 0.7arcs (counts)
FLUX_GAAP_0p7_r	1E	count	GAAP r-band flux minaper 0.7arcs (counts)
FLUX_GAAP_0p7_i	1E	count	GAAP i-band flux minaper 0.7arcs (counts)
FLUXERR_GAAP_0p7_u	1E	count	Error on FLUX_GAAP_u minaper 0.7arcs (counts)
FLUXERR_GAAP_0p7_g	1E	count	Error on FLUX_GAAP_g minaper 0.7arcs (counts)
FLUXERR_GAAP_0p7_r	1E	count	Error on FLUX_GAAP_r minaper 0.7arcs (counts)
FLUXERR_GAAP_0p7_i	1E	count	Error on FLUX_GAAP_i minaper 0.7arcs (counts)
FLAG_GAAP_1p0_u	1J		GAaP Flag for MAG_GAAP_u minaper 1.0arcs
FLAG_GAAP_1p0_g	1J		GAaP Flag for MAG_GAAP_g minaper 1.0arcs
FLAG_GAAP_1p0_r	1J		GAaP Flag for MAG_GAAP_r minaper 1.0arcs
FLAG_GAAP_1p0_i	1J		GAaP Flag for MAG_GAAP_i minaper 1.0arcs
FLUX_GAAP_1p0_u	1E	count	GAAP u-band flux minaper 1.0arcs (counts)
FLUX_GAAP_1p0_g	1E	count	GAAP g-band flux minaper 1.0arcs (counts)
FLUX_GAAP_1p0_r	1E	count	GAAP r-band flux minaper 1.0arcs (counts)
FLUX_GAAP_1p0_i	1E	count	GAAP i-band flux minaper 1.0arcs (counts)
FLUXERR_GAAP_1p0_u	1E	count	Error on FLUX_GAAP_u minaper 1.0arcs (counts)
FLUXERR_GAAP_1p0_g	1E	count	Error on FLUX_GAAP_g minaper 1.0arcs (counts)
FLUXERR_GAAP_1p0_r	1E	count	Error on FLUX_GAAP_r minaper 1.0arcs (counts)
FLUXERR_GAAP_1p0_i	1E	count	Error on FLUX_GAAP_i minaper 1.0arcs (counts)
MAG_GAAP_0p7_u	1E	mag	u-band GAaP magnitude min_aper=0.7arcsec
MAGERR_GAAP_0p7_u	1E	mag	u-band GAaP magnitude error min_aper=0.7arcsec
MAG_GAAP_0p7_g	1E	mag	g-band GAaP magnitude min_aper=0.7arcsec
MAGERR_GAAP_0p7_g	1E	mag	g-band GAaP magnitude error min_aper=0.7arcsec
MAG_GAAP_0p7_r	1E	mag	r-band GAaP magnitude min_aper=0.7arcsec
MAGERR_GAAP_0p7_r	1E	mag	r-band GAaP magnitude error min_aper=0.7arcsec
MAG_GAAP_0p7_i	1E	mag	i-band GAaP magnitude min_aper=0.7arcsec
MAGERR_GAAP_0p7_i	1E	mag	i-band GAaP magnitude error min_aper=0.7arcsec
MAG_GAAP_1p0_u	1E	mag	u-band GAaP magnitude min_aper=1.0arcsec
MAGERR_GAAP_1p0_u	1E	mag	u-band GAaP magnitude error min_aper=1.0arcsec
MAG_GAAP_1p0_g	1E	mag	g-band GAaP magnitude min_aper=1.0arcsec
MAGERR_GAAP_1p0_g	1E	mag	g-band GAaP magnitude error min_aper=1.0arcsec
MAG_GAAP_1p0_r	1E	mag	r-band GAaP magnitude min_aper=1.0arcsec
MAGERR_GAAP_1p0_r	1E	mag	r-band GAaP magnitude error min_aper=1.0arcsec
MAG_GAAP_1p0_i	1E	mag	i-band GAaP magnitude min_aper=1.0arcsec
MAGERR_GAAP_1p0_i	1E	mag	i-band GAaP magnitude error min_aper=1.0arcsec
Suppementary Source Parameters from THELI r-band Detection Image			
MAG_ISO	1E	mag	r-band Isophotal Magnitude (mag)
MAGERR_ISO	1E	mag	Error on MAG_ISO (mag)
FLUX_ISO	1E	count	r-band Isophotal Flux (counts)
FLUXERR_ISO	1E	count	Error on FLUX_ISO (counts)
MAG_ISOCOR	1E	mag	r-band Corrected Isophotal Magnitude (mag)
MAGERR_ISOCOR	1E	mag	Error on MAG_ISOCOR (mag)
FLUX_ISOCOR	1E	count	r-band Corrected Isophotal Flux (counts)
FLUXERR_ISOCOR	1E	count	Error on FLUX_ISOCOR (counts)
NIMAFLAGS_ISO	1I		Number of flagged pixels over the isophotal profile

IMAFLAGS_ISO	1I		FLAG-image flags ORed over the isophotal profile
XMIN_IMAGE	1I	pixel	Minimum x-coordinate among detected pixels (pixel)
YMIN_IMAGE	1I	pixel	Minimum y-coordinate among detected pixels (pixel)
XMAX_IMAGE	1I	pixel	Maximum x-coordinate among detected pixels (pixel)
YMAX_IMAGE	1I	pixel	Maximum x-coordinate among detected pixels (pixel)
X_WORLD	1D	deg	Barycentre position along world x axis (deg)
Y_WORLD	1D	deg	Barycentre position along world y axis (deg)
X2_WORLD	1E	deg**2	Variance of position along X_WORLD (alpha) (deg^2)
Y2_WORLD	1E	deg**2	Variance of position along X_WORLD (delta) (deg^2)
XY_WORLD	1E	deg**2	Covariance of position X_WORLDY_WORLD (deg^2) /
ERRX2_WORLD	1E	deg**2	Error on XY_WORLD (deg^2)
ERRY2_WORLD	1E	deg**2	Error on XY_WORLD (deg^2)
ERRXY_WORLD	1E	deg**2	Error on XY_WORLD (deg^2)
CXX_WORLD	1E	deg**(-2)	SExtractor Cxx object ellipse parameter (deg^-2)
CYY_WORLD	1E	deg**(-2)	SExtractor Cyy object ellipse parameter (deg^-2)
CXY_WORLD	1E	deg**(-2)	SExtractor Cxy object ellipse parameter (deg^-2)
ERRCXX_WORLD	1E	deg**(-2)	Error on CXX_WORLD (deg^-2)
ERRCYY_WORLD	1E	deg**(-2)	Error on CYY_WORLD (deg^-2)
ERRCXY_WORLD	1E	deg**(-2)	Error on CXY_WORLD (deg^-2)
A_IMAGE	1D	pixel	Profile RMS along x-axis (pix)
B_IMAGE	1D	pixel	Profile RMS along y-axis (pix)
ERRA_IMAGE	1E	pixel	Error on A_IMAGE
ERRB_IMAGE	1E	pixel	Error on B_IMAGE
S_ELLIPTICITY	1E		SExtractor Ellipticity (1-B_IMAGEA_IMAGE) /
S_ELONGATION	1E		SExtractor Elongation (A_IMAGEB_IMAGE) /
MAG_APER_4	1E	mag	r-band Magnitude within a circular aperture of 4 pixels (mag)
MAGERR_APER_4	1E	mag	Error on MAG_APER_4 (mag)
FLUX_APER_4	1E	count	r-band Flux within a circular aperture of 4 pixels (counts)
FLUXERR_APER_4	1E	count	Error on FLUX_APER_4 (counts)
MAG_APER_6	1E	mag	r-band Magnitude within a circular aperture of 6 pixels (mag)
MAGERR_APER_6	1E	mag	Error on MAG_APER_6 (mag)
FLUX_APER_6	1E	count	r-band Flux within a circular aperture of 6 pixels (counts)
FLUXERR_APER_6	1E	count	Error on FLUX_APER_6 (counts)
MAG_APER_8	1E	mag	r-band Magnitude within a circular aperture of 8 pixels (mag)
MAGERR_APER_8	1E	mag	Error on MAG_APER_8 (mag)
FLUX_APER_8	1E	count	r-band Flux within a circular aperture of 8 pixels (counts)
FLUXERR_APER_8	1E	count	Error on FLUX_APER_8 (counts)
MAG_APER_10	1E	mag	r-band Magnitude within a circular aperture of 10 pixels (mag)
MAGERR_APER_10	1E	mag	Error on MAG_APER_10 (mag)
FLUX_APER_10	1E	count	r-band Flux within a circular aperture of 10 pixels (counts)
FLUXERR_APER_10	1E	count	Error on FLUX_APER_10 (counts)
MAG_APER_14	1E	mag	r-band Magnitude within a circular aperture of 14 pixels (mag)
MAGERR_APER_14	1E	mag	Error on MAG_APER_14 (mag)
FLUX_APER_14	1E	count	r-band Flux within a circular aperture of 14 pixels (counts)
FLUXERR_APER_14	1E	count	Error on FLUX_APER_14 (counts)
MAG_APER_20	1E	mag	r-band Magnitude within a circular aperture of 20 pixels (mag)
MAGERR_APER_20	1E	mag	Error on MAG_APER_20 (mag)
FLUX_APER_20	1E	count	r-band Flux within a circular aperture of 20 pixels (counts)

FLUXERR_APER_20	1E	count	Error on FLUX_APER_20 (counts)
MAG_APER_30	1E	mag	r-band Magnitude within a circular aperture of 30 pixels (mag)
MAGGERR_APER_30	1E	mag	Error on MAG_APER_30 (mag)
FLUXERR_APER_30	1E	count	r-band Flux within a circular aperture of 30 pixels (counts)
FLUX_APER_30	1E	count	Error on FLUX_APER_30 (counts)
MAG_APER_40	1E	mag	r-band Magnitude within a circular aperture of 40 pixels (mag)
MAGERR_APER_40	1E	mag	Error on MAG_APER_40 (mag)
FLUX_APER_40	1E	count	r-band Flux within a circular aperture of 40 pixels (counts)
FLUXERR_APER_40	1E	count	Error on FLUX_APER_40 (counts)
MAG_APER_60	1E	mag	r-band Magnitude within a circular aperture of 60 pixels (mag)
MAGERR_APER_60	1E	mag	Error on MAG_APER_60 (mag)
FLUX_APER_60	1E	count	r-band Flux within a circular aperture of 60 pixels (counts)
FLUXERR_APER_60	1E	count	Error on FLUX_APER_60 (counts)
MAG_APER_100	1E	mag	r-band Magnitude within a circular aperture of 100 pixels (mag)
MAGERR_APER_100	1E	mag	Error on MAG_APER_100 (mag)
FLUX_APER_100	1E	count	r-band Flux within a circular aperture of 100 pixels (counts)
FLUXERR_APER_100	1E	count	Error on FLUX_APER_100 (counts)
ISO0	1I	pixel**2	Isophotal area at level 0 (pixel^2)
ISO1	1I	pixel**2	Isophotal area at level 1 (pixel^2)
ISO2	1I	pixel**2	Isophotal area at level 2 (pixel^2)
ISO3	1I	pixel**2	Isophotal area at level 3 (pixel^2)
ISO4	1I	pixel**2	Isophotal area at level 4 (pixel^2)
ISO5	1I	pixel**2	Isophotal area at level 5 (pixel^2)
ISO6	1I	pixel**2	Isophotal area at level 6 (pixel^2)
ISO7	1I	pixel**2	Isophotal area at level 7 (pixel^2)
ALPHA_J2000	1D	deg	SExtractor named Centroid sky position right ascension (J2000) (deg)
DELTA_J2000	1D	deg	SEXtractor named Centroid sky position declination (J2000) (deg)
SG2DPHOT	1I		2DPhot StarGalaxy classifier (1 for high confidence star)
HTM	1J		Hierarchical Triangular Mesh (level 25)
FIELD_POS	1I		Reference number to field parameters
THELI_NAME	14A		Name of the pointing in THELI convention
KIDS_TILE	14A		Name of the pointing in AW convention
GAaP photometry parametes from the VIKING Z,Y,J,H,Ks pawprints			
EXTINCTION_Z	1E	mag	Galactic extinction in the Z band (mag)
EXTINCTION_Y	1E	mag	Galactic extinction in the Y band (mag)
EXTINCTION_J	1E	mag	Galactic extinction in the J band (mag)
EXTINCTION_H	1E	mag	Galactic extinction in the H band (mag)
EXTINCTION_Ks	1E	mag	Galactic extinction in the Ks band (mag)
MAG_GAAP_0p7_Z	1E	mag	Z magnitude
MAGERR_GAAP_0p7_Z	1E	mag	Z magnitude error
FLUX_GAAP_0p7_Z	1E	count	Z flux
FLUXERR_GAAP_0p7_Z	1E	count	Z flux error
FLAG_GAAP_0p7_Z	1I		GAAP photometry Flag
MAG_GAAP_1p0_Z	1E	mag	Z magnitude
MAGERR_GAAP_1p0_Z	1E	mag	Z magnitude error
FLUX_GAAP_1p0_Z	1E	count	Z flux
FLUXERR_GAAP_1p0_Z	1E	count	Z flux error

FLAG_GAAP_1p0_Z	1I		GAAP photometry Flag
MAG_GAAP_0p7_Y	1E	mag	Y magnitude
MAGERR_GAAP_0p7_Y	1E	mag	Y magnitude error
FLUX_GAAP_0p7_Y	1E	count	Y flux
FLUXERR_GAAP_0p7_Y	1E	count	Y flux error
FLAG_GAAP_0p7_Y	1I		GAAP photometry Flag
MAG_GAAP_1p0_Y	1E	mag	Y magnitude
MAGERR_GAAP_1p0_Y	1E	mag	Y magnitude error
FLUX_GAAP_1p0_Y	1E	count	Y flux
FLUXERR_GAAP_1p0_Y	1E	count	Y flux error
FLAG_GAAP_1p0_Y	1I		GAAP photometry Flag
MAG_GAAP_0p7_J	1E	mag	J magnitude
MAGERR_GAAP_0p7_J	1E	mag	J magnitude error
FLUX_GAAP_0p7_J	1E	count	J flux
FLUXERR_GAAP_0p7_J	1E	count	J flux error
FLAG_GAAP_0p7_J	1I		GAAP photometry Flag
MAG_GAAP_1p0_J	1E	mag	J magnitude
MAGERR_GAAP_1p0_J	1E	mag	J magnitude error
FLUX_GAAP_1p0_J	1E	count	J flux
FLUXERR_GAAP_1p0_J	1E	count	J flux error
FLAG_GAAP_1p0_J	1I		GAAP photometry Flag
MAG_GAAP_0p7_H	1E	mag	H magnitude
MAGERR_GAAP_0p7_H	1E	mag	H magnitude error
FLUX_GAAP_0p7_H	1E	count	H flux
FLUXERR_GAAP_0p7_H	1E	count	H flux error
FLAG_GAAP_0p7_H	1I		GAAP photometry Flag
MAG_GAAP_1p0_H	1E	mag	H magnitude
MAGERR_GAAP_1p0_H	1E	mag	H magnitude error
FLUX_GAAP_1p0_H	1E	count	H flux
FLUXERR_GAAP_1p0_H	1E	count	H flux error
FLAG_GAAP_1p0_H	1I		GAAP photometry Flag
MAG_GAAP_0p7_Ks	1E	mag	Ks magnitude
MAGERR_GAAP_0p7_Ks	1E	mag	Ks magnitude error
FLUX_GAAP_0p7_Ks	1E	count	Ks flux
FLUXERR_GAAP_0p7_Ks	1E	count	Ks flux error
FLAG_GAAP_0p7_Ks	1I		GAAP photometry Flag
MAG_GAAP_1p0_Ks	1E	mag	Ks magnitude
MAGERR_GAAP_1p0_Ks	1E	mag	Ks magnitude error
FLUX_GAAP_1p0_Ks	1E	count	Ks flux
FLUXERR_GAAP_1p0_Ks	1E	count	Ks flux error
FLAG_GAAP_1p0_Ks	1I		GAAP photometry Flag
Optimal aperture 9-band GaaP photometry			
MAG_GAAP_u	1E	mag	u-band GAaP magnitude optimal min_aper
MAGERR_GAAP_u	1E	mag	u-band GAaP magnitude error optimal min_aper
FLUX_GAAP_u	1E	count	u-band GAaP flux optimal min_aper
FLUXERR_GAAP_u	1E	count	u-band GAaP flux error optimal min_aper
FLAG_GAAP_u	1I		GAaP Flag for MAG_GAAP_u optimal min_aper
MAG_GAAP_g	1E	mag	g-band GAaP magnitude optimal min_aper

MAGERR_GAAP_g	1E	mag	g-band GAaP magnitude error optimal min_aper
FLUX_GAAP_g	1E	count	g-band GAaP flux optimal min_aper
FLUXERR_GAAP_g	1E	count	g-band GAaP flux error optimal min_aper
FLAG_GAAP_g	1I		GAaP Flag for MAG_GAAP_g optimal min_aper
MAG_GAAP_r	1E	mag	r-band GAaP magnitude optimal min_aper
MAGERR_GAAP_r	1E	mag	r-band GAaP magnitude error optimal min_aper
FLUX_GAAP_r	1E	count	r-band GAaP flux optimal min_aper
FLUXERR_GAAP_r	1E	count	r-band GAaP flux error optimal min_aper
FLAG_GAAP_r	1I		GAaP Flag for MAG_GAAP_r optimal min_aper
MAG_GAAP_i	1E	mag	i-band GAaP magnitude optimal min_aper
MAGERR_GAAP_i	1E	mag	i-band GAaP magnitude error optimal min_aper
FLUX_GAAP_i	1E	count	i-band GAaP flux optimal min_aper
FLUXERR_GAAP_i	1E	count	i-band GAaP flux error optimal min_aper
FLAG_GAAP_i	1I		GAaP Flag for MAG_GAAP_i optimal min_aper
MAG_GAAP_Z	1E	mag	Z-band GAaP magnitude optimal min_aper
MAGERR_GAAP_Z	1E	mag	Z-band GAaP magnitude error optimal min_aper
FLUX_GAAP_Z	1E	count	Z-band GAaP flux optimal min_aper
FLUXERR_GAAP_Z	1E	count	Z-band GAaP flux error optimal min_aper
FLAG_GAAP_Z	1I		GAaP Flag for MAG_GAAP_Z optimal min_aper
MAG_GAAP_Y	1E	mag	Y-band GAaP magnitude optimal min_aper
MAGERR_GAAP_Y	1E	mag	Y-band GAaP magnitude error optimal min_aper
FLUX_GAAP_Y	1E	count	Y-band GAaP flux optimal min_aper
FLUXERR_GAAP_Y	1E	count	Y-band GAaP flux error optimal min_aper
FLAG_GAAP_Y	1I		GAaP Flag for MAG_GAAP_Y optimal min_aper
MAG_GAAP_J	1E	mag	J-band GAaP magnitude optimal min_aper
MAGERR_GAAP_J	1E	mag	J-band GAaP magnitude error optimal min_aper
FLUX_GAAP_J	1E	count	J-band GAaP flux optimal min_aper
FLUXERR_GAAP_J	1E	count	J-band GAaP flux error optimal min_aper
FLAG_GAAP_J	1I		GAaP Flag for MAG_GAAP_J optimal min_aper
MAG_GAAP_H	1E	mag	H-band GAaP magnitude optimal min_aper
MAGERR_GAAP_H	1E	mag	H-band GAaP magnitude error optimal min_aper
FLUX_GAAP_H	1E	count	H-band GAaP flux optimal min_aper
FLUXERR_GAAP_H	1E	count	H-band GAaP flux error optimal min_aper
FLAG_GAAP_H	1I		GAaP Flag for MAG_GAAP_H optimal min_aper
MAG_GAAP_Ks	1E	mag	Ks-band GAaP magnitude optimal min_aper
MAGERR_GAAP_Ks	1E	mag	Ks-band GAaP magnitude error optimal min_aper
FLUX_GAAP_Ks	1E	count	Ks-band GAaP flux optimal min_aper
FLUXERR_GAAP_Ks	1E	count	Ks-band GAaP flux error optimal min_aper
FLAG_GAAP_Ks	1I		GAaP Flag for MAG_GAAP_Ks optimal min_aper
Agaper	1E	arcsec	Major axis of GAaP aperture optimal min_aper (arcsec)
Bgaper	1E	arcsec	Minor axis of GAaP aperture optimal min_aper (arcsec)
Photometric redshift estimate			
Z_B	1D		9-band BPZ redshift estimate; peak of posterior probability distribution
Z_B_MIN	1D		Lower bound of the 68% confidence interval of Z_B
Z_B_MAX	1D		Upper bound of the 68% confidence interval of Z_B
T_B	1D		Spectral type corresponding to Z_B
ODDS	1D		Empirical ODDS of Z_B

Z_ML	1D		9-band BPZ maximum likelihood redshift
T_ML	1D		Spectral type corresponding to Z_ML
CHI_SQUARED_BPZ	1D		chi sqared value associated with Z_B
M_0	1D	mag	Reference magnitude for BPZ prior
BPZ_FILT	1J		filters with good photometry (BPZ)
NBPZ_FILT	1J		number of filters with good phot. (BPZ)
BPZ_NONDETFILT	1J		filters with faint photometry (BPZ)
NBPZ_NONDETFILT	1J		number of filters with faint phot. (BPZ)
BPZ_FLAGFILT	1J		flagged filters (BPZ)
NBPZ_FLAGFILT	1J		number of flagged filters (BPZ)
MASK	1J		9-band mask information (see table 9 for important note)
Extinction-corrected colours			
COLOUR_GAAP_u_g	1E	mag	u-g colour index
COLOUR_GAAP_g_r	1E	mag	g-r colour index
COLOUR_GAAP_r_i	1E	mag	r-i colour index
COLOUR_GAAP_i_Z	1E	mag	i-Z colour index
COLOUR_GAAP_Z_Y	1E	mag	Z-Y colour index
COLOUR_GAAP_Y_J	1E	mag	Y-J colour index
COLOUR_GAAP_J_H	1E	mag	J-H colour index
COLOUR_GAAP_H_Ks	1E	mag	H-Ks colour index

Table 8. MASK values in the 9-band catalogues (see Table 9 for important note)

Bit	Meaning
0	THELI manual mask (very conservative)
1	THELI automatic large star halo mask (faint)
2	THELI automatic large star halo mask (bright) or bright star mask
3	Manual mask of regions around globular clusters, Fornax dwarf, ISS passage
4	THELI void mask, or asteroids, or weight=0
5	VIKING Z band image masked (see Table 9 for important note)
6	VIKING Y band image masked (see Table 9 for important note)
7	VIKING J band image masked (see Table 9 for important note)
8	VIKING H band image masked (see Table 9 for important note)
9	VIKING Ks band image masked (see Table 9 for important note)
10	Astro-WISE u band halo+stellar PULECENELLA mask or weight=0
11	Astro-WISE g band halo+stellar PULECENELLA mask or weight=0
12	Astro-WISE r band halo+stellar PULECENELLA mask or weight=0
13	Astro-WISE i band halo+stellar PULECENELLA mask or weight=0
14	Object outside the RA/DEC cut for its tile
15	Not used (reserved as sign bit in FITS 2-byte integer)

Table 9. List of affected tiles for which the multiband mask image, and the MASK parameter in the multiband catalogue, were incorrect in DR4.0 , and have been corrected in DR4.1 .

KIDS_0.0_-28.2	KIDS_170.0_1.5	KIDS_206.0_-1.5	KIDS_236.0_-1.5
KIDS_0.0_-29.2	KIDS_170.5_2.5	KIDS_206.6_-2.5	KIDS_236.7_2.5
KIDS_0.0_-30.2	KIDS_170.5_-2.5	KIDS_207.0_1.5	KIDS_237.0_1.5
KIDS_0.0_-31.2	KIDS_171.0_1.5	KIDS_207.0_-1.5	KIDS_237.0_-1.5
KIDS_0.0_-32.1	KIDS_171.5_-2.5	KIDS_208.0_1.5	KIDS_237.7_2.5
KIDS_0.0_-33.1	KIDS_187.5_2.5	KIDS_208.0_-1.5	KIDS_24.0_-34.1
KIDS_0.0_-34.1	KIDS_187.5_-2.5	KIDS_209.0_1.5	KIDS_24.5_-31.2
KIDS_0.0_-35.1	KIDS_188.0_1.5	KIDS_209.0_-1.5	KIDS_24.7_-32.1
KIDS_13.8_-30.2	KIDS_188.5_2.5	KIDS_209.6_2.5	KIDS_25.2_-34.1
KIDS_157.0_1.5	KIDS_189.0_1.5	KIDS_210.0_1.5	KIDS_28.8_-34.1
KIDS_157.0_-1.5	KIDS_189.5_2.5	KIDS_210.0_-1.5	KIDS_30.5_-28.2
KIDS_157.4_2.5	KIDS_190.0_1.5	KIDS_220.6_-3.5	KIDS_31.6_-28.2
KIDS_157.4_-2.5	KIDS_190.5_2.5	KIDS_221.6_-3.5	KIDS_329.5_-28.2
KIDS_158.0_1.5	KIDS_191.0_1.5	KIDS_225.0_1.5	KIDS_329.7_-27.2
KIDS_158.0_-1.5	KIDS_191.5_2.5	KIDS_225.0_-1.5	KIDS_32.7_-28.2
KIDS_158.4_2.5	KIDS_192.0_1.5	KIDS_225.6_2.5	KIDS_330.8_-27.2
KIDS_158.4_-2.5	KIDS_192.5_2.5	KIDS_226.0_1.5	KIDS_331.8_-28.2
KIDS_159.0_1.5	KIDS_193.0_1.5	KIDS_226.0_-1.5	KIDS_332.0_-27.2
KIDS_159.0_-1.5	KIDS_193.5_2.5	KIDS_226.6_2.5	KIDS_332.9_-28.2
KIDS_159.4_2.5	KIDS_194.0_1.5	KIDS_227.0_1.5	KIDS_334.0_-28.2
KIDS_159.4_-2.5	KIDS_194.5_2.5	KIDS_227.0_-1.5	KIDS_334.2_-27.2
KIDS_160.0_1.5	KIDS_195.5_2.5	KIDS_227.6_2.5	KIDS_335.2_-28.2
KIDS_160.0_-1.5	KIDS_196.0_1.5	KIDS_228.0_1.5	KIDS_336.3_-28.2
KIDS_160.4_2.5	KIDS_196.5_2.5	KIDS_228.0_-1.5	KIDS_337.4_-28.2
KIDS_161.0_1.5	KIDS_197.0_1.5	KIDS_228.6_2.5	KIDS_337.6_-27.2
KIDS_161.0_-1.5	KIDS_197.5_2.5	KIDS_229.0_1.5	KIDS_338.6_-28.2
KIDS_161.4_2.5	KIDS_198.0_1.5	KIDS_229.0_-1.5	KIDS_339.7_-28.2
KIDS_161.4_-2.5	KIDS_198.6_2.5	KIDS_22.1_-31.2	KIDS_33.9_-28.2
KIDS_162.0_1.5	KIDS_199.0_1.5	KIDS_22.6_-33.1	KIDS_340.8_-28.2
KIDS_163.0_1.5	KIDS_199.6_2.5	KIDS_22.8_-34.1	KIDS_343.1_-28.2
KIDS_163.0_-1.5	KIDS_1.1_-28.2	KIDS_230.0_1.5	KIDS_345.3_-28.2
KIDS_164.0_1.5	KIDS_200.0_1.5	KIDS_230.0_-1.5	KIDS_346.5_-28.2
KIDS_164.0_-1.5	KIDS_200.6_2.5	KIDS_230.6_2.5	KIDS_348.7_-28.2
KIDS_165.0_1.5	KIDS_200.6_-2.5	KIDS_231.0_1.5	KIDS_349.8_-28.2
KIDS_165.0_-1.5	KIDS_201.0_1.5	KIDS_231.0_-1.5	KIDS_351.0_-28.2
KIDS_166.0_1.5	KIDS_201.6_2.5	KIDS_231.6_2.5	KIDS_352.1_-28.2
KIDS_166.5_2.5	KIDS_201.6_-2.5	KIDS_232.0_1.5	KIDS_353.2_-28.2
KIDS_167.0_1.5	KIDS_202.0_1.5	KIDS_232.0_-1.5	KIDS_354.4_-28.2
KIDS_167.0_-1.5	KIDS_202.6_2.5	KIDS_232.6_2.5	KIDS_355.5_-28.2
KIDS_167.5_2.5	KIDS_202.6_-2.5	KIDS_233.0_1.5	KIDS_356.6_-28.2
KIDS_167.5_-2.5	KIDS_203.0_1.5	KIDS_233.0_-1.5	KIDS_358.9_-28.2
KIDS_168.0_1.5	KIDS_203.6_2.5	KIDS_233.6_2.5	KIDS_36.1_-28.2
KIDS_168.0_-1.5	KIDS_204.0_1.5	KIDS_234.0_1.5	KIDS_37.2_-28.2
KIDS_168.5_2.5	KIDS_204.0_-1.5	KIDS_234.0_-1.5	KIDS_39.5_-28.2
KIDS_168.5_-2.5	KIDS_204.6_-2.5	KIDS_234.7_2.5	KIDS_40.6_-28.2
KIDS_169.0_1.5	KIDS_205.0_1.5	KIDS_235.0_1.5	KIDS_41.8_-28.2
KIDS_169.0_-1.5	KIDS_205.0_-1.5	KIDS_235.0_-1.5	KIDS_44.0_-28.2
KIDS_169.5_2.5	KIDS_205.6_2.5	KIDS_235.7_2.5	KIDS_4.5_-28.2
KIDS_169.5_-2.5	KIDS_206.0_1.5	KIDS_236.0_1.5	KIDS_5.6_-28.2

Acknowledgements

The following acknowledgment is valid at the moment of writing this document. For an up-to-date version, please visit the following webpage:
http://kids.strw.leidenuniv.nl/DR4/acknowledgements.php

Users of data from this release should cite “Kuijken et al. (2019), A&A 625, A2”. (The publication is available at https://doi.org/10.1051/0004-6361/201834918)

Please use the following statement in your articles when using these data:

Based on observations made with ESO Telescopes at the La Silla Paranal Observatory under programme IDs 177.A-3016, 177.A-3017, 177.A-3018 and 179.A-2004, and on data products produced by the KiDS consortium. The KiDS production team acknowledges support from: Deutsche Forschungsgemeinschaft, ERC, NOVA and NWO-M grants; Target; the University of Padova, and the University Federico II (Naples).